Study of n-WO3/p-porous silicon structures for gas-sensing applications

H. Mhamdi, R. Benabderrahmane Zaghouani, T. Fiorido, J.-L. Lazzari, Marc Bendahan, W. Dimassi

▶ **To cite this version:**

H. Mhamdi, R. Benabderrahmane Zaghouani, T. Fiorido, J.-L. Lazzari, Marc Bendahan, et al.. Study of n-WO3/p-porous silicon structures for gas-sensing applications. Journal of Materials Science: Materials in Electronics, 2020, 31 (10), pp.7862-7870. 10.1007/s10854-020-03324-8 . hal-02867069

HAL Id: hal-02867069
https://amu.hal.science/hal-02867069

Submitted on 24 Feb 2021

HAL is a multi-disciplinary open access archive for the deposit and dissemination of scientific research documents, whether they are published or not. The documents may come from teaching and research institutions in France or abroad, or from public or private research centers.

L'archive ouverte pluridisciplinaire **HAL**, est destinée au dépôt et à la diffusion de documents scientifiques de niveau recherche, publiés ou non, émanant des établissements d'enseignement et de recherche français ou étrangers, des laboratoires publics ou privés.

Study of n-WO_3/p-porous silicon structures for gas sensing applications

H. Mhamdi[1,5], R. Benabderrahmane Zaghouani[1*], T. Fiorido[2], J.-L. Lazzari[3], M. Bendahan[2], W. Dimassi[4]

[1]*Laboratoire de Photovoltaïque, Centre de Recherches et des Technologies de l'Energie, Technopôle de Borj-Cédria, BP, 95 Hammam-Lif, Tunis, Tunisie*

[2] *Aix Marseille Univ, Université de Toulon, CNRS, IM2NP, Marseille, France*

[3]*Aix Marseille Université, CNRS, CINaM UMR 7325,*

Campus de Luminy, Case 913, 163, Avenue de Luminy, 13288 Marseille Cedex 09, France

[4]*Laboratoire de Nanomatériaux et Systèmes pour Energies Renouvelables, Centre de Recherches et des Technologies de l'Energie, Technopôle de Borj-Cédria, BP, 95 Hammam-Lif, Tunis, Tunisie*

[5]*Faculté des sciences de Tunis, Université Tunis El Manar, 2092 Tunis, Tunisia.*

[*]Corresponding author: Rabia Benabderrahmane

Tel.:+216 96148416; Fax: +216 79325825

E-mail address: rabia.benabderrahmane@gmail.com

Abstract

In this work, we report on the gas sensing properties of n-WO_3/p-porous silicon (PS) structures. Nanostructured WO_3 films are deposited by simple chemical method via dip-coating of PS in tungsten hexachloride solution. The morphological and structural properties of the elaborated structures were investigated using Atomic Force Microscope (AFM), Raman and Fourier Transform Infrared (FTIR) Spectrometers. The NO_2-sensing performances of the sensor were measured at different operating temperatures ranging from room temperature to 250 °C, different NO_2 concentrations and different time exposure. The sensor showed a p-type semiconducting behavior which probably owning to the strong effect of the hetero-junction between the n-WO_3 nanoparticles and p-porous silicon substrate. The obtained results confirm the suitability of these structures to detect low NO_2 concentrations up to 1 ppm at moderate temperatures. These sensors exhibit fast response and recovery times.

Keywords:

Tungsten oxide, Porous silicon, NO_2 detection response time, recovery time

I. Introduction

During last decades, there has been an increasing demand for high-performance gas detection systems to be used in various fields such as environment monitoring, automotive and pharmaceutical industries. There is a permanent quest for reduced sizes, high-throughput and cost-effectiveness sensors. In particular, sensors based on metal-oxide semiconductors (MOX) have been extensively studied offering low cost, high stability, and compatibility with microelectronic technology. The most studied MOX are titanium dioxide (TiO_2) [1], zinc oxide (ZnO) [2], Tin oxide (SnO_2) [3], molybdenum oxide (MoO_3) [4], and tungsten oxide (WO_3) [5]. These materials, with interesting physical and chemical properties, exhibit a resistive response to different gases. In fact, they present naturally non-stoichiometric structures [6] attributed to oxygen vacancies leading to a semiconductor behavior [7]. The operating principle of a MOX sensor is based on the adsorption of oxidizing or reducing molecules on the surface of the sensitive layer leading to its conductivity increase or reduction respectively. Currently, in the most developed sensors, the sensitive layers are generally deposited on an insulator layer with a transducer permitting their heating at an optimal temperature and the resistance measurement. Many solutions are proposed to improve the MOX sensors performance such as structuring the sensitive layer, which considerably increases the number of adsorption sites. In this work, a way of improvement could be reached by increasing the porosity and the active surface of the oxide, which can be obtained by using a porous silicon substrate. Porous silicon, with its large specific surface area, can form a new generation of gas sensors with semiconductor oxides. Initially developed in the "Silicon On Insulator (SOI)" technology, porous silicon (PS) is pushed back to the research scene as 'the miracle material' after the rediscovery of its photoluminescence at room temperature by Canham in 1990 [8]. In addition to its photoluminescence, porous silicon can act as an antireflection (ARC) layer with low reflectivity in the visible spectrum by trapping light in its pores. Its optoelectronic properties could be modulated by porosity and thickness [9].

In particular, tungsten oxide may form with porous silicon an interesting gas sensor. It is considered as n-type semiconductor with a band gap around 3 eV. This multifunctional material combines many features: good chemical stability in aqueous solutions, outstanding electrochromic, photochromic and photocatalytic properties [10-12]. WO_3 could be elaborated by different techniques such as: chemical vapor deposition [10, 13], spray pyrolysis [14], sol gel [15], electrodeposition [16] and atomic layer deposition (ALD) [17]. In the literature, WO_3 used in gas sensors has been reported in different forms as nanowires [18-19], nanoparticles [20], thin films [21] permitting the detection of different gases: nitrogen dioxide (NO_2) [20-21], hydrogen sulfide (H_2S) [22], ozone (O_3) [23], hydrogen [24], ethanol [24]. The WO_3-based sensor response at an operating temperature is depending strongly on the substrate [21] and the microstructure features [25].

In this work, we propose the use of porous silicon as a substrate for WO_3 deposition. This work highlights an original study with a focus on the NO_2 detection performance of n-WO_3/p-porous silicon hetero-junction obtained by simple chemical methods.

II. Experimental details :

1. Samples preparation :

Porous silicon samples were elaborated by stain etching method in a (HF, HNO_3, H_2O)= (1, 2, 3) in volumetric ratio solution for 2 min using solar grade boron-doped single crystalline silicon substrates (100) with a resistivity of ~1-3 Ω.cm and a thickness of 200 µm. Silicon substrates were successively dipped in boiling acetone for 10

min, in ethanol for 5 min and deionized water in order to eliminate organic greases and metallic surface contaminants. Substrates were then immersed in 10 % acid hydrofluoric for 1 min to eliminate the native oxide, rinsed in deionized water and dried with nitrogen.

After formation of PS layers, substrates were dip-coated for 10 s in a solution containing tungsten hexachloride (WCl_6) to deposit WO_3 layers. The WO_3 solution with a concentration of 0.035 mol/L was prepared using WCl_6 powder, 50 % ethanol and 50 % water under stirring for 3 h at ambient temperature. Finally, the solution was stored in air during 7 days before being used [26-27].

2. Samples characterization:

The WO_3 deposition was analyzed using a Fourier Transform Infrared (FTIR) Nicolet MAGNA-IR 560 Spectrometer and a Raman "LabRAM HR JOBIN YVO Technology HORIBA Scientific" spectrometer at room temperature under the excitation of a 632 nm He–Ne laser. The samples morphology was interpreted by a digital instrument Nanoscope 3100 Atomic Force Microscopy (AFM). The surface reflectivity was measured by a PerkinElmer Lambda 950 UV/VIS/NIR spectrometer equipped with an integrating sphere. Photoluminescence (PL) analysis was done by home-made equipment with a 447 nm laser.

3. Gas sensing measurement:

To perform electrical measurements, aluminum (Al) parallel electrodes, with a thickness of about 100 nm, were deposited by thermal evaporation system on samples surface. The gas-sensing performances of the n-WO_3/p-PS sensors were evaluated in a static gas sensing testing system, shown in Fig.1 (a). The sensor was placed on a heating plate connected to a temperature controller used to adjust the operating temperature. The sensor dynamic response was obtained by measuring the sensor resistance change under gas. Fig.1 (b-c) present a schematic illustration of the proposed sensor composed of Al/WO_3/PS structure and its photography showing the Al electrodes and the different dimensions.

In this work, the gas sensor response is defined by the following equation (Eq. 1):

$$S = \frac{R_a - R_g}{R_a}.100 \qquad \text{(Eq. 1)}$$

Where R_a and R_g are respectively the sensor resistance measured in air and under gas.

The sensor performance is also described by the response and recovery times. The response time is defined as the time required for the resistance to reach 90 % of the total value change after gas exposure. Accordingly, recovery time is the time necessary for the resistance to return to 10 % above initial resistance after the gas removal.

III. Results and discussion:

1. Porous silicon characterization:

The porous silicon layer is formed by etching the silicon substrate in an acidic solution. The stain-etching process is composed of two chemical reactions as proposed by Robbins and Schwartz [28]. The first reaction leads to the surface oxidation by the nitric acid as described by the equation (Eq. 2):

$$3Si + 4HNO_3 \rightarrow 3SiO_2 + 4NO + 2H_2O \qquad \text{(Eq.2)}$$

In a second step, the formed silicon dioxide is etched by the HF (Eq. 3):

$$SiO_2 + 6HF \rightarrow H_2SiF_6 + 2H_2O \qquad \text{(Eq. 3)}$$

The overall reaction is described by (Eq. 4):

$$3Si + 4\,HNO_3 + 18\,HF \rightarrow 3\,H_2SiF_6 + 4NO + 8H_2O \qquad \text{(Eq. 4)}$$

This etching technique leads to the formation of porous silicon layer.

The porous silicon FTIR absorption spectrum is presented in Fig.2 (a). We distinguish the principal recorded vibration bands: SiH_x stretching mode at 2112 cm^{-1}, Si-O-Si stretching mode at 1092 cm^{-1}, SiH_2 scissors mode at 907 cm^{-1}, Si-Si stretching mode at 628 cm^{-1}, SiH_n wagging mode at 672.7 cm^{-1} and O-SiH_x wagging mode at 861 cm^{-1} [26].

In Fig. 2 (b), porous silicon and silicon substrate reflectivities are compared. A large decrease in the reflectivity of PS (about 5% in the visible) is obtained. Indeed, PS is known for its ability to trap light in the pores thus decreasing the reflections and increasing the light absorption probability within the active region.

Due to its indirect band gap, the silicon emits weak infrared photoluminescence however the porous silicon exhibits a high visible photoluminescence at ambient temperature [8]. Fig. 2(c) shows the PS sample photoluminescence spectrum performed in the wavelength range of (480 nm–750 nm) at room temperature attributed to the nanometric size crystalline structures.

2. WO_3 deposition on porous silicon surface:

Porous silicon, with its high specific surface, will play the role of a template for the WO_3 deposition. In order to study the deposition, a comparison of the FTIR spectra of PS and WO_3/PS samples was done (Fig.3 (a)). The two spectra show almost the same bands with a clearly reduction of SiH_x and Si-O-Si peaks intensities for the WO_3/PS sample suggesting the replacement of H atoms by WO_3 molecules [26]. After zooming different zones (A, B, C) in the spectral region (400 cm^{-1}-1000 cm^{-1}) and the deconvolution of different peaks, the W-O bands are depicted.

The deconvolution of the peak around 906 cm^{-1} in the zone A (Fig.3 (b)) shows peaks at 927.7 cm^{-1} and 898.9 cm^{-1} corresponding to W═O and W-O-W bridging modes respectively [29-30]. The peaks deconvolution in the zone B (Fig.3 (c)) shows a band at 782.9 cm^{-1} attributed to W–O_{intra}–W bridging stretch mode [31]. In the zone C (Fig.3 (d)), the peak at 466 cm^{-1} is describing the W-O_{intra} deformational mode.

Although some peaks could be ascribed to W-O-W and W=O bridging modes, FTIR does not fully evidence the layers chemical composition. That's why Raman analysis was performed. The Raman spectrum of WO_3/PS sample is presented in Fig.4. A principal Raman peak observed at 520 cm^{-1} is attributed to the scattering of the first order optical phonon of c-Si. As reported in the literature, two Raman bands characterizing WO_x, are located in (200-500 cm^{-1}) and (600-1000 cm^{-1}) spectral regions associated to O-W-O bending vibration modes and O-W-O stretching vibration modes respectively. In the WO_3/PS sample Raman spectrum, we notice the presence of two weak broad bands centered at 335 cm^{-1} and 900 cm^{-1} characterizing the amorphous nature and assigned to bending and stretching vibration modes of the monoclinic WO_3 [24].

The PS surface modification by the WO_3 deposition was also studied by AFM. The 3D AFM topographies of the PS and WO_3/PS samples are presented in Fig.5 (a-b). Comparing the two AFM images, we notice a slight modification of PS surface morphology after WO_3 treatment. The untreated PS layer containing pores is considered as an adhesive surface for the WO_3 after immersing wafers into the WCl_6 solution. The WO_3 deposition is noticed by the roughness changes which varied from 132 nm to about 220 nm for PS and WO_3/PS sample respectively.

3. Gas sensing properties:

Fig.6 depicts the WO_3/SP structure resistance variation under dry air at different temperatures. As noticed, the resistance is decreasing with temperature increase. The resistance evolution is thermally activated presenting two different slopes attributed to the existence of two different mechanisms. As reported for metal oxides [32], these mechanisms are essentially the thermal excitation of electrons and oxygen adsorption.

The WO_3/PS sensor is exposed to 4 ppm of NO_2, with humidity of 0%, at different temperatures ranging from room temperature to 250 °C in order to determine the optimal operating temperature. Fig.7 shows the gas sensor responses as a function of the operating temperature. For ambient temperature, no response is obtained. As is commonly known, the WO_3-based sensors are working at high temperatures exceeding 300 °C. The WO_3/PS sensor proposed in this work exhibits a response which initially increased from 50 °C to 100 °C then it decreased. The best response of 40% is obtained for an operating temperature of 100 ° C. In addition, the response and recovery times are measured for the different operating temperatures as displayed in Table 1. The obtained values are low and comparable to those reported in the literature [33]. The recovery time is enhanced with the temperature increase as the gas molecules desorption is promoted at higher temperature. The best response time is obtained at the optimal operating temperature (100 °C). The time-dependent resistance evolution at 100 °C for two consecutive cycles is shown in Fig. 8. It is noticed that this sensor exhibits a good repeatability as a function of time.

Further measurements were performed for lower NO_2 concentrations (1 to 3 ppm) during an exposure time of 1 min (Fig. 9 (a)) at the operating temperature of 100 °C. As we can notice, a sensor response is obtained up to 1 ppm of NO_2. The response increases from 10 % to 20 % for gas concentration varying from 1 to 3 ppm respectively because the sensor is exposed to more gas. The sensor was also exposed to 4 ppm of NO_2 during different exposure times (1 to 3 min). As shown in Fig. 9 (b), the response increases with a total recovery of the resistance in each measurement.

The resistance evolution shows also that the sensor resistance decreases when injecting the gas which is contrary to the typical tungsten oxide sensors. In fact, WO_3 behaving as n-type semiconductor shows an increase of its electrical resistance when exposed to an oxidizing gas such as NO_2. However, the obtained p-type behavior may be attributed to the porous silicon substrate. In order to determine exactly where the conductivity occurs when injecting the gas, porous silicon sensor without WO_3 deposition was tested under 4 ppm of NO_2. Fig. 10 shows the PS resistance response exposed to 4 ppm of NO_2 at 30 °C which is the optimal operating temperature for this sensor. This result already confirms that the porous silicon presence justifies the optimal operating temperature decrease in the WO_3/PS sensor. It can also be seen from the time-dependent resistance evolution that PS sensor displays good signal repeatability in addition to a good return to the initial resistance value showing good reversibility. The crucial remark is that the observed p-type behavior is attributed to the porous silicon.

According to previous works [9], we have shown that the substrate surface is not completely covered by tungsten oxide deposited by the proposed chemical method. So, the injected gas interacts with the PS surface as well as with the WO_3 nanostructures. These nanostructures form a hetero-junction with porous silicon in which appears a potential barrier created by the work functions difference of the two materials. Moreover, it has been shown that, in addition to oxygen adsorption, the interface density of states at the porous layer surface play an important role in the NO_2 detection. In fact, the porous silicon has H-terminated surface which is chemically unstable due

to its formation mechanism leading to the appearance of dangling bonds in ambient conditions. Indeed, the reduction or the oxidation of the surface influences the interface density of states and thus the carrier concentration in the PS surface.

The gas selectivity is an important key parameter to evaluate the gas sensor performance. The WO_3/PS sensor is exposed to reducing and oxidizing gases at 100 °C during 1 min: 100 ppm NH_3, 4 ppm NO_2, 200 ppb O_3, and 20 ppm CO. The sensor response S is defined as:

$$S = \frac{R_g}{R_a} \quad \text{for reducing gases} \qquad \text{(Eq. 5)}$$

And as $S = \frac{R_a}{R_g}$ for oxidizing gases (Eq. 6)

Where R_g and R_a are the sensor resistance under gas and in the air, respectively.

The responses are presented in Fig. 11 (a). As noticed, the elaborated WO_3/PS sensor detects all the exposed gases except the CO. In the literature, there are still problems to detect some gases such as CO, CO_2, SO_2 and more research is needed to establish a better selectivity. The obtained responses are comparable. In order to determine the best gas to detect, the response and recovery times are measured. As shown in Fig 11 (b), the recovery times are very high in the case of NH_3 and O_3 (45 and 9 min, respectively). However, for NO_2, the sensor exhibits the lowest response and recovery times. Therefore, we can consider that the presented sensor is more adapted to detect NO_2.

IV. Conclusions:

In summary, the n-WO_3/p-porous silicon structure was prepared for NO_2 sensing. A simple and low-cost chemical method was proposed to deposit WO_3 nanostructures on porous silicon substrate. It was found that the prepared sensors are promising for NO_2 sensing with low concentrations. Fourier transform infrared spectroscopy analysis shows that WO_3/PS sample presents peaks ascribed to O-W-O and W=O bridging bonds. Raman spectrum of the WO_3/PS sample presents two weak broad bands centered at 335 cm^{-1} and 900 cm^{-1} characterizing the amorphous nature and assigned to bending and stretching vibration modes of the monoclinic WO_3. AFM analysis shows changes in the surface roughness which varied from 132 nm for PS sample to about 220 nm for the WO_3/PS sample. These sensors present fast response and recovery times at a moderate temperature (100 °C). Despite these interesting results, a further amelioration of these sensors is necessary. In particular, a better control of the oxide deposition by the amelioration of the porous silicon surface could be reached by using electrochemical etching method.

Acknowledgements:

This work was supported by the Tunisian Ministry of Higher Education and Scientific Research.

Conflict of Interest Statement:

The authors declare that they have no conflict of interest

References

[1] B. Comert Sertel, N. Akin Sonmez, M. Donmez Kaya, S. Ozcelik, Development of MgO:TiO_2 thin films for gas sensor applications, Ceram. Int. 45 (2019) 2917.

[2] R. Moraes Oliveira, M. S. Vieira, M. N. F. Silva, Enhancement of acetylene gas sensing properties for ZnO-based gas sensor produced by plasma immersion ion implantation and deposition, Mater. Sci. Semicond. Process. 93 (2019) 339.

[3] M. S. Barbosa, P. H. Suman, J. J. Kim, H. L. Tuller, M. O. Orlandi, Investigation of electronic and chemical sensitization effects promoted by Pt and Pd nanoparticles on Single-crystalline SnO nanobelt-based gas sensors, Sens. Actuators, B 301 (2019) 127055.

[4] X. Fu, P. Yang, X. Xiao, D. Zhou, R. Huang, X. Zhang, F. Cao, J. Xiong, Y. Hu, Y. Tu, Y. Zou, Z. Wang, H. Gu, Ultra-fast and highly selective room-temperature formaldehyde gas sensing of Pt-decorated MoO_3 nanobelts, J. Alloys Compd. 797 (2019) 666.

[5] M. Yin, L. Yu, S. Liu, Synthesis of Ag quantum dots sensitized WO_3 nanosheets and their enhanced acetone sensing properties, Mater. Lett. 186 (2017) 66.

[6] J. Kaur, R. Kumar and M.C. Bhatnagar, Effect of indium-doped SnO_2 nanoparticles on NO_2 gas sensing properties, Sens. Actuators, B 126 (2007) 478.

[7] P.S. Shewale, V. B. Patil, S. W. Shin, J. H. Kim and M.D. Uplane, H_2S gas sensing properties of nanocrystalline Cu-doped ZnO thin films prepared by advanced spray pyrolysis, Sens. Actuators, B 186 (2013) 226.

[8] L. T. Canham, Silicon quantum wire array fabrication by electrochemical and chemical dissolution of wafers, Appl. Phys. Lett. 57(1990) 1046.

[9] R. B. Zaghouani, M. Alaya, H. Nouri, J.-L. Lazzari, W. Dimassi, Study of WO_3-decorated porous silicon and Al_2O_3-ALD encapsulation, J. Mater. Sci.:Mater. Electron. 29 (2018) 17731.

[10] C. S. Blackman, I. P. Parkin, Atmospheric Pressure Chemical Vapor Deposition of Crystalline Monoclinic WO_3 and WO_{3-x} Thin Films from Reaction of WCl_6 with O-Containing Solvents and Their Photochromic and Electrochromic Properties, Chem. Mater. 17 (2005) 1583.

[11] C. Gomez-Solis, D. Sanchez-Martinez, I. Juarez-Ramirez, A. Martinez-de la Cruz, L. M. Torres Martinez, Facile synthesis of m-WO_3 powders via precipitation in ethanol solution and evaluation of their photocatalytic activities, J. Photochem. Photobiol. A. 262 (2013) 28.

[12] C. C. Liao, F. R. Chen, J. J. Kai, Electrochromic properties of nanocomposite WO_3 films, Sol. Energy Mater. Sol. Cells. 91 (2007) 1282.

[13] R. G. Gordona, S. Barry, J. T. Barton, R.N.R. Broomhall-Dillard, Atmospheric pressure chemical vapor deposition of electrochromic tungsten oxide films, Thin Solid Films. 392 (2001) 231.

[14] C. P. Li, C.A. Wolden, A. C. Dillon, R. C. Tenent, Electrochromic films produced by ultrasonic spray deposition of tungsten oxide nanoparticles, Sol. Energy Mater. Sol. Cells. 99 (2012) 50.

[15] N. Sharma, M. Deepa, P. Varshney, S.A. Agnihotry, FTIR and absorption edge studies on tungsten oxide based precursor materials synthesized by sol–gel technique, J. Non-Cryst. Solids 306 (2002) 129.

[16] A. J. More, R. S. Patil, D. S. Dalavi, S. S. Mali, C. K. Hong, M. G. Gang, J. H. Kim, and P. S. Patil, Electrodeposition of nano-granular tungsten oxide thin films for smart window application, Mat. Lett. 134 (2014) 298.

[17] J. Malm, T. Sajavaara, M. Karppinen, Atomic layer deposition of WO_3 thin films using $W(CO)_6$ and O_3 precursors, Chem. Vap. Deposition 18 (2012) 245.

[18] W. Yan, M. Hu, J. Liang, D. Wang, Y. Wei, W. Zhang, Y. Qin, Preparation and room temperature NO2-sensing performances of n-porous silicon/n-WO_3 nanowires heterojunction, Mater. Res. Bull. 83 (2016) 453.

[19] D. F. Wang, J.R. Liang, C.Q. Li, W. J. Yan, M. Hu, Room temperature NO_2 gas sensing of Au-loaded tungsten oxide nanowires/porous silicon hybrid structure, Chin. Phys. B 25 (2016) 028102.

[20] W. Yan, M. Hu, P. Zeng, S. Ma, M. Li, Room temperature NO_2-sensing properties of WO_3 nanoparticles/porous silicon, Appl. Surf. Sci. 292 (2014) 551.

[21] D.S. Lee, K.H. NAM, D. D. Lee, Effect of substrate on NO_2-sensing properties of WO_3 thin film gas sensors, Thin Solid Films 375 (2000) 142.

[22] B. Urasinska-Wojcik, T.A. Vincent, J.W. Gardner, H_2S sensing properties of WO_3 based gas sensor, Procedia Eng. 168 (2016) 255.

[23] M. Gillet, K. Aguir, M. Bendahan, P. Mennini, Grain size effect in sputtered tungsten trioxide thin films on the sensitivity to ozone, Thin Solid Films 484 (2005) 358.

[24] M. Ahsan, T.Tesfamichael, J. Bell, W. Wlodarski, N. Motta, Low Temperature Response of Nanostructured Tungsten Oxide Thin Films towards Hydrogen and Ethanol, Sens. and Actuators, B 173(2012) 789.

[25] M. Li, M. Hu, D. Jia, S. Ma, W. Yan, NO_2-sensing properties based on the nanocomposite of n-WO_{3-x}/n-porous silicon at room temperature, Sens. and Actuators, B 186 (2013) 140.

[26] M. Alaya, R. B. Zaghouani, S. Khamlich, J. L. Lazzari, W. Dimassi, Enhancement of physical properties of stain-etched porous silicon by integration of WO_3 nanoparticles, Thin Solid Films 645(2018) 51.

[27] S. Badilescu, P.V. Ashrit, Study of sol-gel prepared nanostructured WO_3 thin films and composites for electrochromic applications, Solid State Ionics 158 (2002) 187.

[28] H. Robbins, B. Schwartz, Chemical Etching of Silicon, J. Electrochem. Soc. 106 (1959) 505.

[29] J. Diaz-Reyes, V. Dorantes-Garcia, A. Pérez-Benitez, J. A. Baderas-Lopez, Obtaining of films of tungsten trioxide (WO_3) by resistive heating of a tungsten filament, Superf. Vacio. 21 (2008) 12.

[30] M. Deepa, M. Kar, S.A. Agnihotry, Electrodeposited tungsten oxide films: annealing effects on structure and elechtrochromic performance, Thin Solid Films 468(2004) 32.

[31] N. Mendoza-Aguero, V. Agarwal, Optical and structural characterization of tungsten oxide electrodeposited on nanostructured porous silicon: effect of annealing atmosphere and temperature, J. Alloys Compd. 581 (2013) 596.

[32] I. Madhi, M. Saadoun, B. Bessais, Sensing characteristics of zinc oxide thin films deposited by spray pyrolysis onto tubular Pyrex substrate, Mater. Sci. Semicond. Process. 16(2013) 1365.

[33] B. Urasinska-Wojcik, T.A. Vincent, M. F. Ghowdhury, J.W. Gardner, ultrasensitive WO_3 gas sensors for NO2 detection in air and low oxygen environment, Sens. Actuators, B 239 (2017)1051.

Figure Caption

Figure 1: (a) The schematic diagram of the static gas sensing test system (b) Schematic illustration of the sensor (c) Photography of the sensor showing the Al electrodes.

Figure 2: (a) FTIR absorption spectrum of PS sample (b) Reflectivity spectra of silicon and PS samples (c) PL spectrum of PS sample.

Figure 3: FTIR absorption spectra of: (a) PS and WO_3/PS samples, amplification of (b) zone A (c) zone B (d) zone C for the WO_3/PS sample.

Figure 4: Raman spectrum of the WO_3/PS sample.

Figure 5: AFM topographies (a) untreated PS surface (b) WO_3/PS sample.

Figure 6: Sensor resistance variation as a function of the operating temperature in ambient air.

Figure 7: Dynamic response of the WO_3/PS sensor as a function of the operating temperature.

Figure 8: Resistance response of the WO_3/PS sensor exposed to 4 ppm of NO_2 at 100 °C.

Figure 9: (a) WO_3/PS sensor response to different NO_2 concentrations during 1 min at 100 °C (b) Resistance response of the WO_3/PS sensor at 100 °C exposed to 4 ppm of NO_2 during different durations.

Figure 10: Resistance response of the PS sensor exposed to 4 ppm of NO_2 at 30 °C.

Figure 11: (a) WO_3/PS sensor response to 4 ppm of NO_2, 100 ppm NH_3, 200 ppb O_3 at 100 °C (b) The recovery and response times of the WO_3/PS sensor exposed to different gases.

Tables

Table 1: The recovery and response times of the WO_3/PS sensor exposed to 4 ppm of NO_2 at different operating temperatures.

Table 1

Operating temperature (°C)	50	100	150	200	250
Response time (s)	35	25	39	41	45
Recovery time (s)	38	23	19	12	8

Figure 1

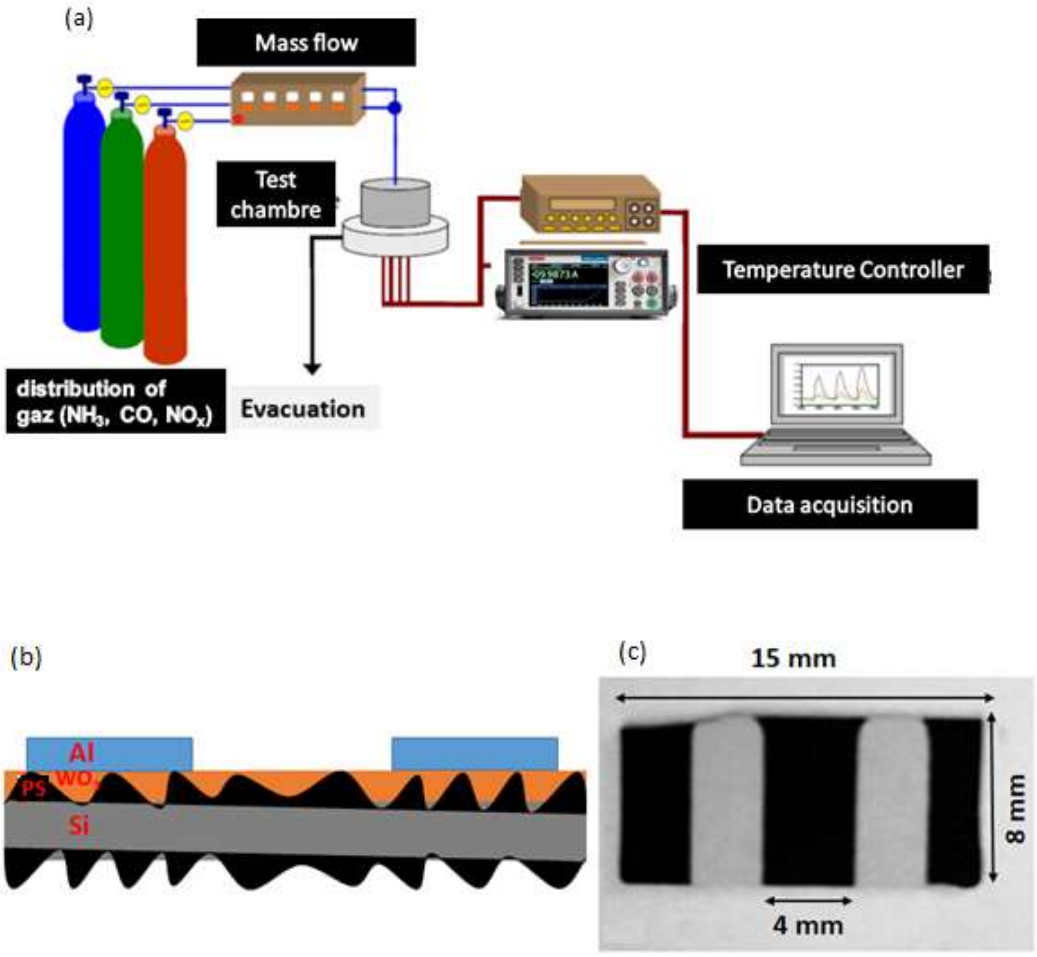
(a)
Mass flow
Test chambre
Temperature Controller
distribution of gaz (NH_3, CO, NO_x)
Evacuation
Data acquisition
(b)
Al
WO
PS
Si
(c)
15 mm
8 mm
4 mm

Figure 2

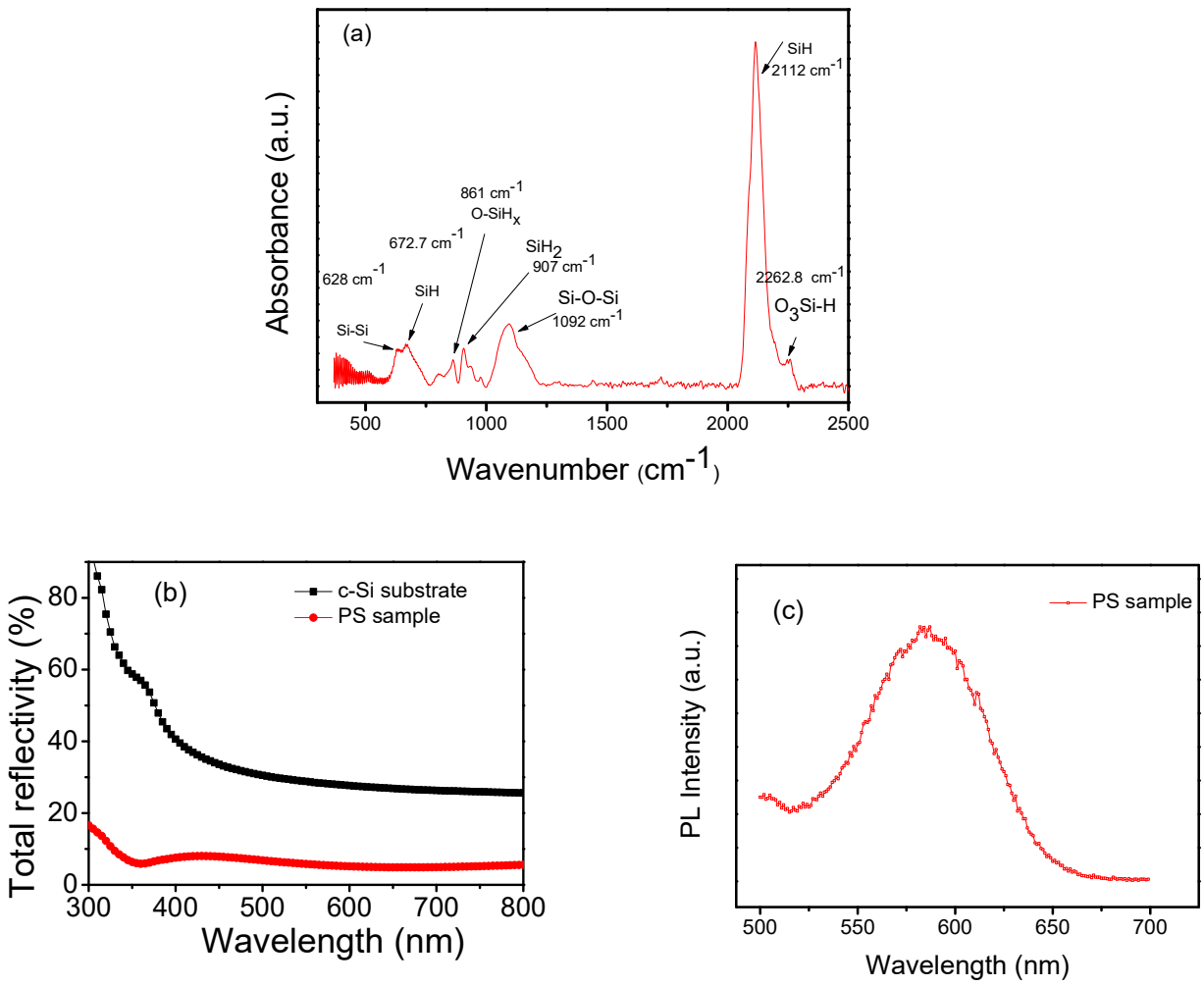
(a)
Absorbance (a.u.)
Wavenumber (cm-1)
Si-Si
628 cm-1
SiH
672.7 cm-1
861 cm-1
O-SiHx
SiH2
907 cm-1
Si-O-Si
1092 cm-1
SiH
2112 cm-1
2262.8 cm-1
O3Si-H
(b)
c-Si substrate
PS sample
Total reflectivity (%)
Wavelength (nm)
(c)
PS sample
PL Intensity (a.u.)
Wavelength (nm)

Figure 3

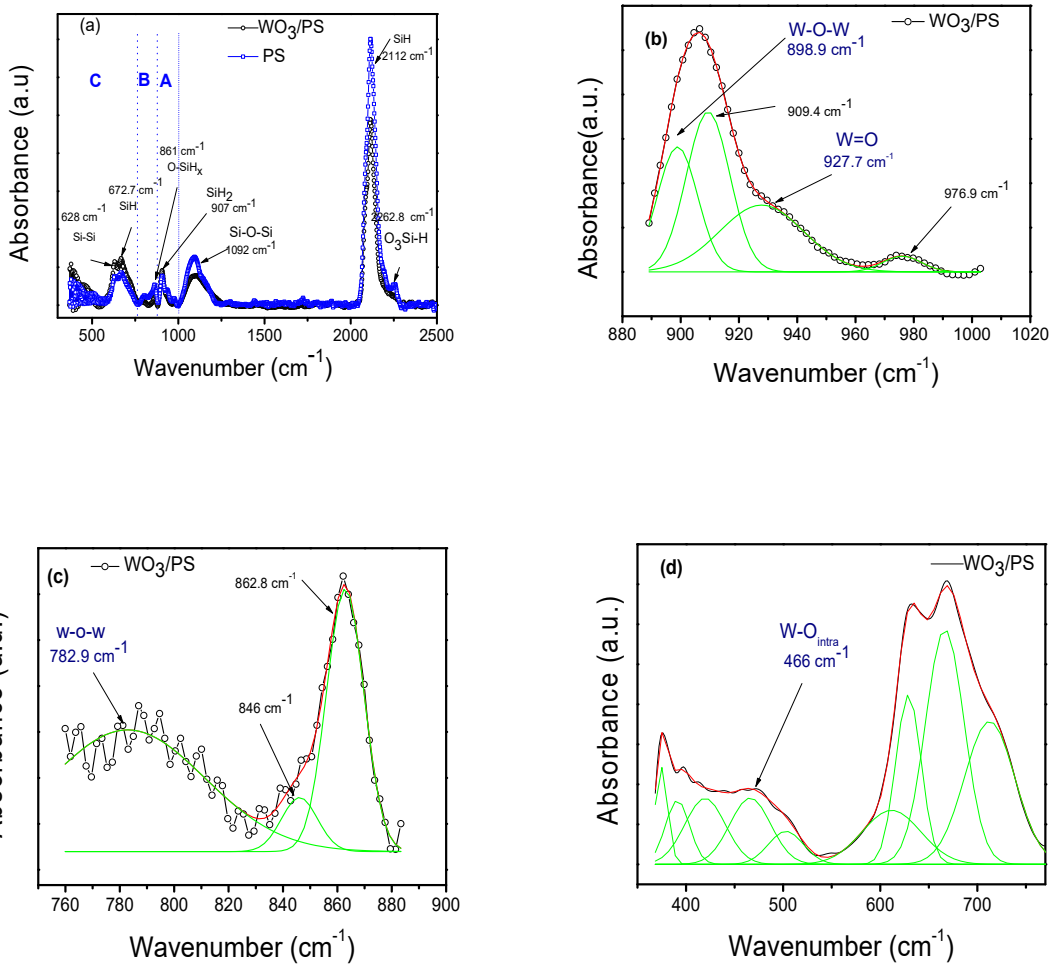
(a)
WO3/PS
PS
C
B
A
SiH
2112 cm-1
861 cm-1
O-SiHx
672.7 cm-1
SiH
628 cm-1
Si-Si
SiH2
907 cm-1
Si-O-Si
1092 cm-1
2262.8 cm-1
O3Si-H
Absorbance (a.u)
Wavenumber (cm-1)
(b)
WO3/PS
W-O-W
898.9 cm-1
909.4 cm-1
W=O
927.7 cm-1
976.9 cm-1
Absorbance(a.u.)
Wavenumber (cm-1)
(c)
WO3/PS
862.8 cm-1
w-o-w
782.9 cm-1
846 cm-1
Absorbance (a.u.)
Wavenumber (cm-1)
(d)
WO3/PS
W-Ointra
466 cm-1
Absorbance (a.u.)
Wavenumber (cm-1)

Figure 4

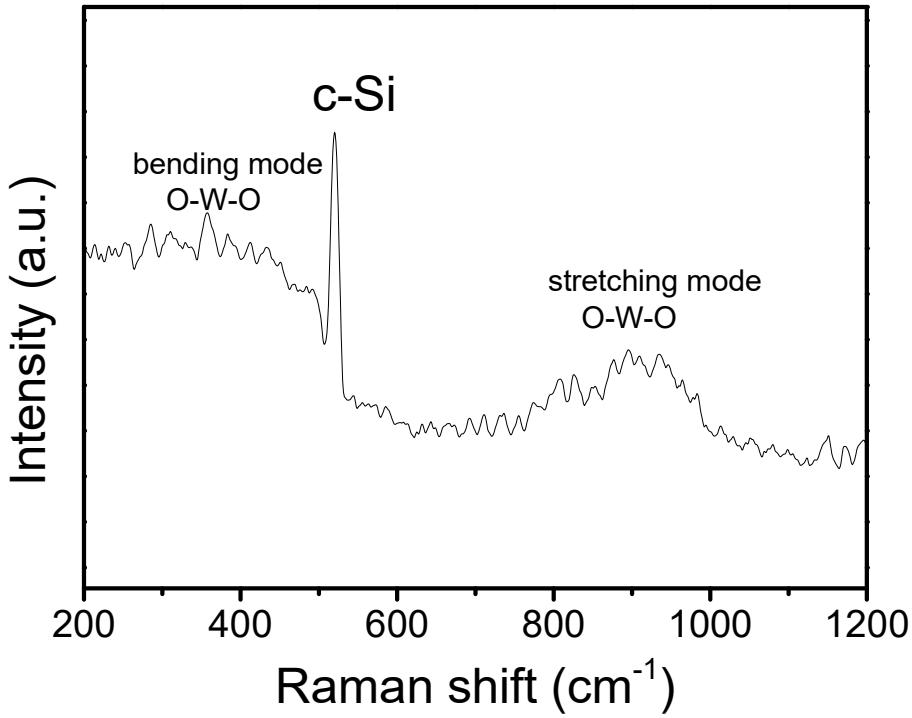
c-Si
bending mode
O-W-O
stretching mode
O-W-O
Intensity (a.u.)
200
400
600
800
1000
1200
Raman shift (cm-1)

Figure 5

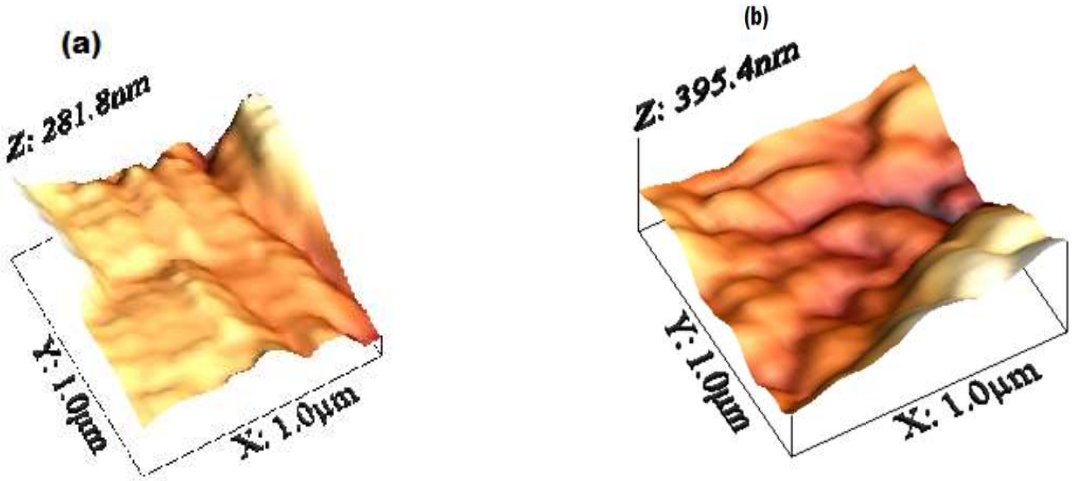

Figure 6

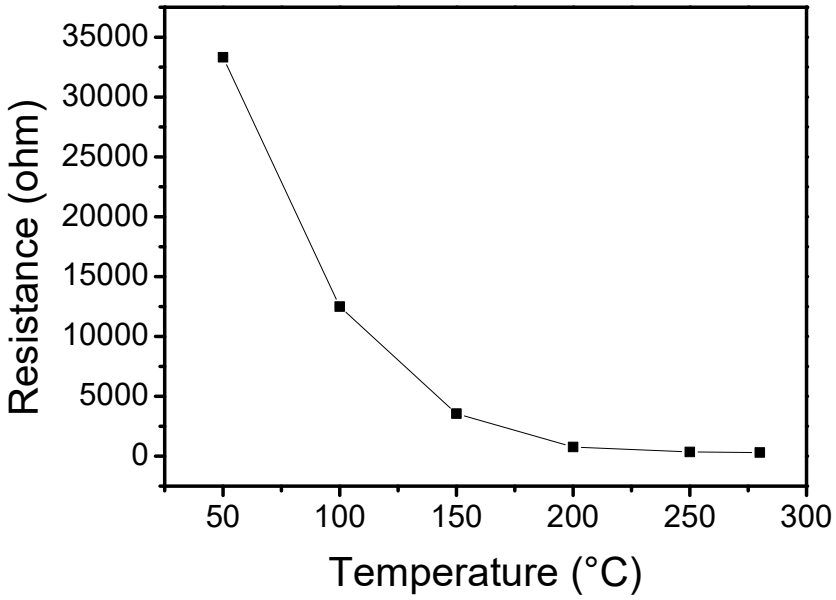
Resistance (ohm)
35000
30000
25000
20000
15000
10000
5000
0
50
100
150
200
250
300
Temperature (°C)

Figure 7

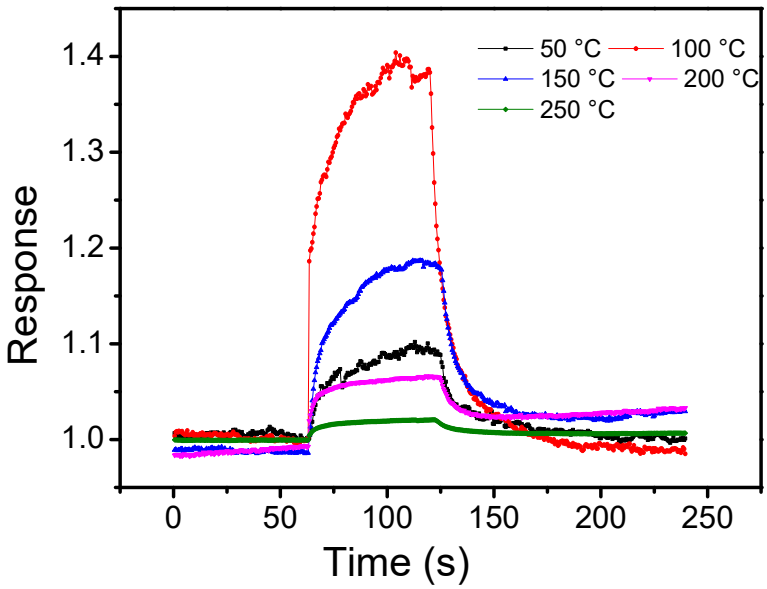
50 °C
100 °C
150 °C
200 °C
250 °C
Response
Time (s)
1.0
1.1
1.2
1.3
1.4
0
50
100
150
200
250

Figure 8

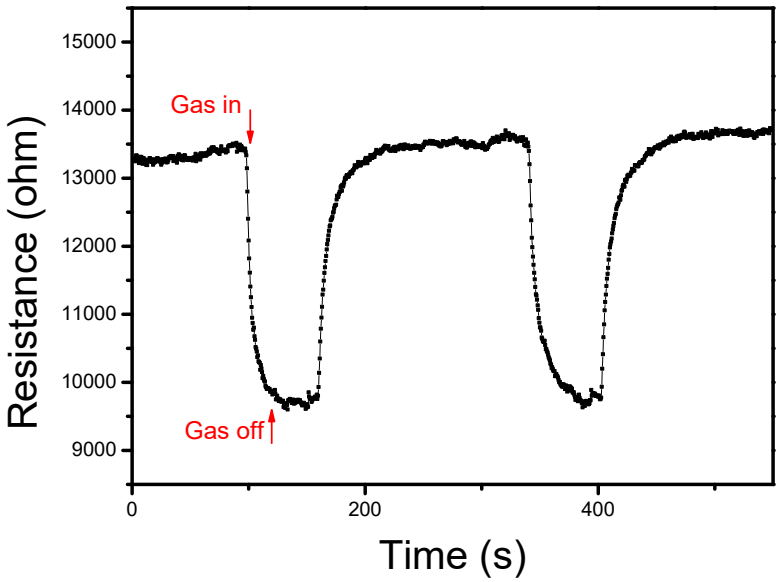
Resistance (ohm)
15000
14000
13000
12000
11000
10000
9000
Gas in
Gas off
0
200
400
Time (s)

Figure 9(a)

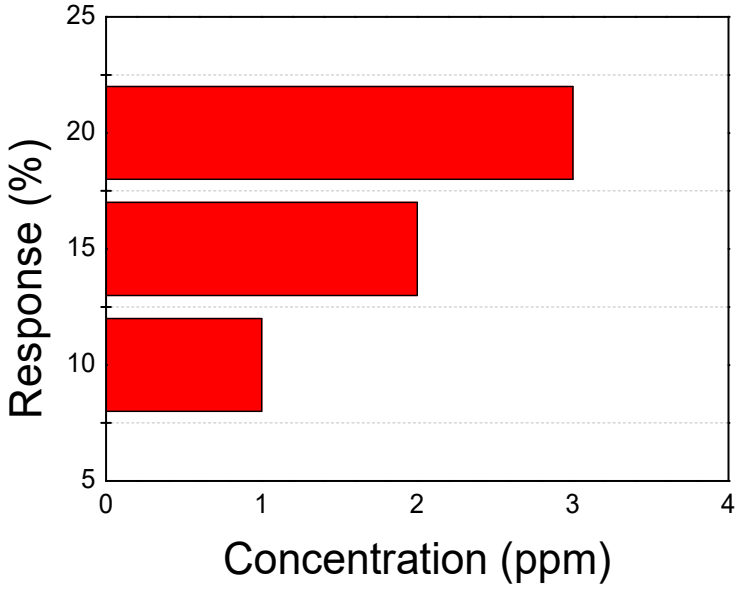

Figure 9(b)

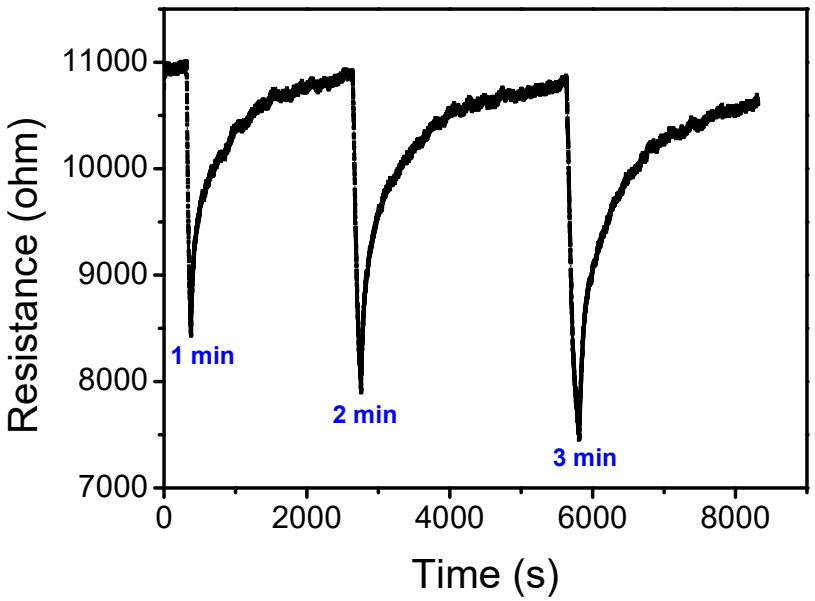

Figure 10

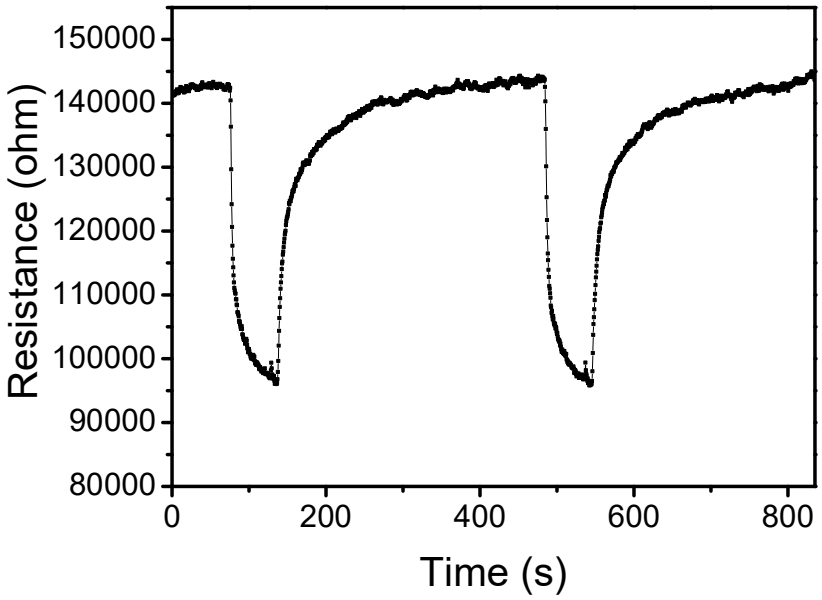
Resistance (ohm)
150000
140000
130000
120000
110000
100000
90000
80000
0
200
400
600
800
Time (s)

Figure 11(a)

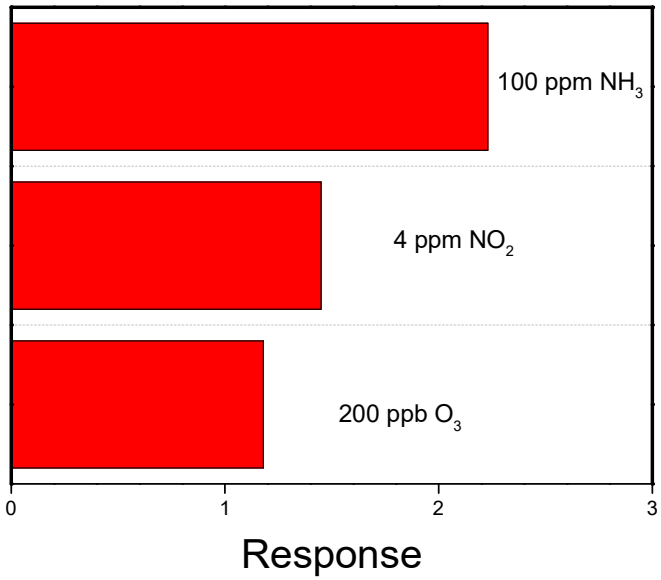

Figure 11(b)